Biomass Conversion and Biorefinery
https://doi.org/10.1007/s13399-025-06745-9

ORIGINAL ARTICLE

Green synthesis of tin and titanium nanoparticles using edible plant extracts: exploring their anticancer and antifungal activities

Mine Sulak[1] · **Berna Kavakcıoğlu Yardımcı**[2,3]

Received: 26 September 2024 / Revised: 27 February 2025 / Accepted: 4 March 2025

Abstract

The rise of green chemistry underscores the need for simple and cost-effective nanomaterial synthesis utilizing plant extracts. In this study, tin (IV) oxide and titanium dioxide nanoparticles (SnO_2NPs and TiO_2NPs) were synthesized through a green method from *Cnicus benedictus* and *Aronia melanocarpa* extracts, respectively. These plant sources were selected due to their rich bioactive content, which enhances nanoparticle synthesis and stability. Besides, the use of these extracts eliminates the need for harmful reducing agents, offering an eco-friendly approach compared to conventional green synthesis methods. Characterization with XRD, ATR-FTIR, and FE-SEM confirmed the successful synthesis. SnO_2NPs had a tetragonal crystal structure with a dimension of 27.48 nm, while the average crystal size of the dominant rutile phase in the structure of TiO_2NPs was 19.88 nm. ATR-FTIR spectra of SnO_2NPs and TiO_2NPs indicated the presence of specific vibration peaks of the O–Sn–O and Ti–O bonds, respectively. While the SnO_2NPs had a spherical structure, the TiO_2NPs did not distribute homogeneously, and there were clustered particles in the structure. Both nanomaterials were found to be effective against the human breast cancer cell line. The cell viability was 43.45% and 49.56% after treatment with SnO_2NPs and TiO_2NPs, respectively. Finally, especially SnO_2NPs but not TiO_2NPs showed anti-proliferative effects on both wild-type *Saccharomyces cerevisiae* BY4741 and *Candida albicans*. These findings indicate the potential applicability of these nanoparticles in biomedicine, particularly for targeted cancer therapies and antifungal treatments, as well as in environmental remediation.

Keywords Nanoparticles · *Cnicus benedictus* · *Aronia melanocarpa* · Green synthesis · Characterization · Biological activity

Highlights
- SnO_2NPs and TiO_2NPs were synthesized by using the green synthesis method.
- The characterization was conducted with XRD, ATR-FTIR, and FE-SEM plus EDX.
- SnO_2NPs and TiO_2NPs exerted anticancer activities against the MCF-7 cell line.
- SnO_2NPs showed promising antifungal activity against *S. cerevisiae and C. albicans.*

✉ Mine Sulak
msulak@pau.edu.tr

✉ Berna Kavakcıoğlu Yardımcı
byardimci@pau.edu.tr

[1] Department of Mathematics and Science Education, Faculty of Education, Science Education, Pamukkale University, Denizli, Turkey

[2] Department of Chemistry, Faculty of Science, Pamukkale University, Denizli, Turkey

[3] Advanced Technology Application and Research Center, Pamukkale University, Denizli, Turkey

1 Introduction

Nanotechnology, a rapidly advancing field, focuses on the synthesis, characterization, modification, and application of nanoparticles (NPs) with dimensions ranging from 1 to 100 nm [1, 2]. The nanoscale size imparts unique physicochemical and biological properties to NPs, distinguishing them significantly from their bulk counterparts [3–5]. There are several developed methods used in the production of NPs, but due to the fact that chemical and physical methods are both expensive technologies and toxic to nature and living things, besides yielding products with low particle stability, the focus of the researchers has shifted towards "biological or green synthesis" [6]. This term implies the synthesis of NPs by using bioactive agents such as plant materials, microorganisms, or various biowastes, which reduces the waste product problem without harmful effects [7]. Additionally, NPs synthesized by green processes often exhibit optimal dimensions that are favorable for specific

Published online: 13 March 2025

applications, such as enhanced surface area-to-volume ratios or improved functionality, due to the efficiency of the single-step synthesis procedure [8, 9]. Such NPs are collectively referred to as biogenic NPs [10]. Especially plants or plant extracts attract more attention, mostly because of their eco-friendly waste products, the availability, and suitability for mass production [11]. Plant-derived materials are cost-effective, do not require special storage conditions, pose no risk of contamination, and exhibit high stability under harsh conditions [12]. Metabolites found in plant extracts, such as ketones, aldehydes, flavones, amides, terpenoids, carboxylic acids, phenols, and ascorbic acids, possess the capability to convert metal salts into metal NPs [13, 14]. NPs that are produced using plant extracts are more stable, and the synthesis rates are higher compared to microorganisms. In addition, they generally exhibit pharmaceutical and nutraceutical properties [15].

The plants *Cnicus benedictus* (also known as Şevketi Bostan) and *Aronia melanocarpa* (also known as black chokeberry) were used to make tin (IV) oxide (SnO_2) and titanium dioxide (TiO_2) NPs (SnO_2NPs and TiO_2NPs) using green synthesis methods for the first time, respectively. As previously mentioned, both plants provide substantial benefits in green synthesis, such as the capacity of plant metabolites, including flavonoids, phenols, and terpenoids, to efficiently stabilize and convert metal salts into NPs with enhanced stability and potential biomedical applications [16, 17]. The utilization of these rich plants, which have been the subject of content analyses in recent years, in nanoparticle synthesis for the first time in this context is highly significant. *Cnicus benedictus* is an edible wild plant that belongs to the *Cnicus* L. genus and *Asteraceae* family. *Aronia melanocarpa* is a shrub-like plant that belongs to the *Rosaceae* family. Chokeberry is an alternative name for this fruit. These species exhibit numerous beneficial impacts on human health, which are likely associated with their rich phytochemical compositions [18–20]. Both SnO_2NPs and TiO_2NPs attract remarkable attention with their unique features and momentous applications. The main features enabling SnO_2NPs to be used in many versatile areas can be listed as strong thermal and chemical stability, a high specific area, a high degree of transparency in the visible spectrum, strong chemical and physical interactions with the adsorbed species, a wide band gap from 3.6 to 3.8 eV, low electrical resistance, and low density [21]. Thanks to these unique features, SnO_2NPs have been applied in critical fields such as gas sensors, solar cells, transparent electrodes, lithium-ion batteries, heat mirrors, glass coatings, and photocatalysis [22, 23]. TiO_2NPs can exist in three distinct phases in the nanoscale range at varying temperatures, namely anatase, rutile, and brookite. These phases have a significant impact on the physical characteristics of the fabricated material [24]. Pigments, adsorbents, catalyst supports, filters, coatings, photoconductors, and dielectric materials are among the primary applications of TiO_2NPs, which have gained widespread recognition as semiconductors with photocatalytic properties in recent years [25–31]. The literature survey indicates that there has been a significant increase in the momentum of research on the green synthesis of SnO_2NPs and TiO_2NPs from plants over the past decade [21, 32]. Importantly, it is clearly seen that ongoing studies are also dealing with the evaluation of the possible biological activities in addition to the purpose of synthesizing NPs in a clean and inexpensive way, which increases the diversity of use in various but especially in medicinal areas. For instance, TiO_2NPs synthesized using plant extracts have been shown to form predominantly in the anatase phase with sizes ranging between 15 and 28 nm, exhibiting excellent photocatalytic and antimicrobial properties. Notably, NPs synthesized in this manner achieved an 87% photodegradation efficiency against methylene blue, a common pollutant, while also demonstrating significant antimicrobial activity, suggesting their potential as an eco-friendly and sustainable solution for water purification and biomedical applications [33]. Similarly, SnO_2NPs synthesized using *Laurus nobilis* L. aqueous extract have shown promising applications, particularly in enhancing the properties of biodegradable materials and providing strong antibacterial effects. Functionalization of these NPs with bioactive compounds, such as cefazolin, further improves their antimicrobial efficacy and broadens their potential applications in biomedical and environmental fields. These findings underscore the versatility and sustainability of green-synthesized metal oxide NPs, emphasizing their role in addressing global challenges like food preservation, water purification, and antimicrobial resistance [34]. This study represents the first report of the synthesis of SnO_2NPs and TiO_2NPs using the green synthesis approach, with *Cnicus benedictus* and *Aronia melanocarpa* serving as plant-based reducing and stabilizing agents. The synthesized NPs were successfully characterized, and their biological activities, including anticancer and antifungal properties, demonstrated promising results. The findings revealed that SnO_2NPs exhibit stronger biological activities compared to TiO_2NPs [32], whose structure predominantly consists of the rutile phase. The rutile phase, a stable crystalline form of TiO_2NPs, may limit its ability to interact with biological systems, potentially explaining its comparatively weaker biological activities. These differences underscore the importance of crystalline phase composition in determining the biological efficacy of NPs, highlighting the need for further optimization of synthesis conditions to tailor their properties for specific biomedical applications. In this context, this study not only highlights the novel application of *Cnicus benedictus* and *Aronia melanocarpa* in the green synthesis of SnO_2NPs and TiO_2NPs but also provides valuable insights into their potential biomedical applications.

2 Material and methods

2.1 Material

All chemicals used in the study were in analytical purity and obtained from Sigma-Aldrich Company (St. Louis, MO) unless otherwise stated. *Cnicus benedictus* and *Aronia melanocarpa* were purchased from local markets in Sirinyer, Izmir (Aktar Baharat), and Cınar, Denizli (Aktar Baharat), respectively. The wild-type *S. cerevisiae* BY4741 (MATa his3Δ1 leu2Δ0 met15Δ0 ura3Δ0) and its isogenic cytosolic catalase T (MATa his3Δ1 leu2Δ0 lys2Δ0 ura3Δ0 CTT1::kanMX4), thioredoxin-disulfide reductase (MATa his3Δ1 leu2Δ0 lys2Δ0 ura3Δ0 TRR2::kanMX4), and glutathione synthase (MATa his3Δ1 leu2Δ0 lys2Δ0 ura3Δ0 GSH2::kanMX4) deletion mutants were obtained from Horizon Discovery (Cambridge, UK). *Candida albicans* ATCC 64548 was kindly obtained from Assist. Prof. Dr. Caner Vural. The MCF-7 cell line was obtained from ATCC (American Type Culture Collection, Manassas, VA, USA).

2.2 Preparation of *Cnicus benedictus* and *Aronia melanocarpa* extracts

Various methods have been modified and used for the preparation of *Cnicus benedictus* extract [35]. Briefly, commercially purchased *Cnicus benedictus* leaves were weighed at approximately 40 g, washed three times with ultrapure water, dried, and then chopped with a blender (Waring Commercial Blender HGB2WTG4) for 15 min. Then, 10 g of powdered *Cnicus benedictus* was weighed, transferred to a beaker, and mixed with 100 mL of ultrapure water (1:10). The mixture was left to stir for 4 h at 70 °C and centrifuged at 10,000 rpm for 20 min. The liquid part was filtered through a Gooch crucible under vacuum and stored at + 4 °C until use.

Aronia melanocarpa fruit was washed and dried under sunlight for approximately 1 week. The dehydrated fruit was subsequently pulverized into a fine powder using a blender. A total of 10 g of powdered dried fruits were combined with 100 mL of pure water and heated to approximately 80 °C for 1 h. Subsequently, the extract that had cooled to room temperature was initially filtered using coarse filter paper, followed by filtration through Whatman No. 1 (55 mm, 180 µm) filter paper to guarantee uniformity. The final extract was stored at + 4 °C for subsequent analyses [36].

2.3 Synthesis of SnO_2 and TiO_2 nanoparticles

The synthesis of SnO_2NPs was carried out by modifying the methods of Hong and Jiang (2018) [37] and Kumar et al. (2018) [38]. Briefly, various concentrations of tin (II) chloride dihydrate ($SnCl_2 \times 2H_2O$) metal salts (0.01, 0.02, 0.05, and 0.1 M) were prepared, and the results indicated that the most favorable outcomes were achieved with 0.1 M solutions in terms of nanoparticle size. After preparing the 0.1 M $SnCl_2.2H_2O$ solution in an Erlenmeyer flask, plant extracts were added in varying ratios of the liquid volumes of aqueous metal oxide to plant extract (1:0.5; 1:1; 1:2; 1:4; 1:8; 1:10 (mL/mL)). Specifically, the smallest nanoparticle sizes were obtained when a 1:0.5 ratio was used for the synthesis of SnO_2 nanoparticles. For the optimized synthesis procedure, 10 mL of *Cnicus benedictus* extract at room temperature was added dropwise to the 0.1 M 5 mL $SnCl_2.2H_2O$ solution. The pH value of the mixture was adjusted to 9.0 with 2 M NaOH, and then the reaction mixture was left to stir for 5 h at 80 °C. At the end of the period, the mixture was transferred to the Falcon tube and centrifuged at 10,000 rpm for 20 min. The powdered sample (pellet) remaining in the Falcon tube was centrifuged at 10,000 rpm for 10 min after the washing steps with ultrapure water and ethyl alcohol. The washed pellets were transferred to the glass container to dry for 24 h at 110 °C. The obtained powder after drying was calcined at 600 °C for 4 h. The powder sample was transferred to a new glass container and stored in the dark at room temperature.

The synthesis of TiO_2NPs was carried out by modifying the methods of Ahmad et al. (2020) [39]. Similarly, various concentrations of titanium tetra isopropoxide $[Ti(OCH(CH_3)_2]_4$ metal salts (0.01, 0.02, 0.05, 0.1 M) were prepared, and the results indicated that the most favorable outcomes were achieved with 0.1 M solutions in terms of nanoparticle size. After preparing the 0.1 M titanium tetra isopropoxide solution in an Erlenmeyer flask, plant extracts were added in varying ratios of the liquid volumes of aqueous metal oxide to plant extract (1:0.5; 1:1; 1:2; 1:4; 1:8; 1:10 (mL/mL)). Specifically, the smallest nanoparticle sizes were obtained when a 1:2 ratio was used for the synthesis of TiO_2NPs. For the optimized synthesis procedure, 100 mL of 0.1 M titanium tetra isopropoxide $[Ti(OCH(CH_3)_2]_4$ solution and 50 mL of *Aronia melanocarpa* extract were mixed using a magnetic stirrer at 500 rpm for 2 h at 80 °C. After 2 h, the solution was transferred to centrifuge tubes and centrifuged at 4000 rpm. The resulting pellet was washed twice with pure water before transferring it to a glass container. The resulting compound was dried at 100 °C for 1 h.

2.4 Spectroscopic and microscopic characterization of SnO_2 and TiO_2 nanoparticles

XRD is a powerful non-destructive technique for characterizing crystalline materials. XRD is the primary characterization method to obtain information on structural properties, such as crystal structure and its phase description, average particle size, crystallinity, and crystal

defects [40]. The Debye–Scherrer formula, given below, is employed to obtain the crystallite size of the crystalline material.

$$D = K\lambda/\beta\cos\theta$$

Here, D is the average crystal size of the nanoparticle, K is a constant value and is generally taken as 0.9, λ is the X-ray wavelength (nm), β is the maximum half-height diffraction resulting from the small crystallite size in radians where the peak width of the peak profile, and θ is the diffraction angle [41, 42].

In order to determine the purity of the structure, crystallization degree, and properties of the phases of the SnO_2NPs and TiO_2NPs, XRD analyses were carried out with an APD 2000 PRO diffractometer (GNR, Novara, Italy) using a Cu anode (40 kV, 30 mA) at Kα radiation (λ = 1.5405 Å), at a rate of 2°/min and with an incidence angle of 5° in the range of $5° < 2\theta < 90°$. The intercrystalline distance (D) were calculated using the Debye–Scherrer formula.

ATR-FTIR enables the structural analysis of the material according to the absorption peaks corresponding to the frequencies formed through the vibrations of the bonds between the atoms of the compounds [43]. An ATR-FTIR device (PerkinElmer Inc., Norwalk, CT) was used to determine the functional groups of both the extract residues obtained after the removal of solvents and the SnO_2NPs and TiO_2NPs obtained by the green synthesis method. Measurements were performed in the wavenumber range of 4000–400 cm^{-1}, with 4 cm^{-1} resolution and 50 scans.

The morphology and elemental analysis of SnO_2NPs and TiO_2NPs which were obtained by the green synthesis were investigated by FE-SEM (Zeiss Supra 40 VP, Oberkochen, Germany) and EDX devices (Quorum Q150R ES, Quorum Technologies Ltd, Lewes, UK), respectively, located at the Advanced Technology Application and Research Center (ILTAM). FE-SEM provides information about the size, shape, and distribution of NPs [44], and EDX is a widely used analytical technique for elemental analysis (containing atoms) or chemical characterization of solid-state samples. SnO_2NPs and TiO_2NPs were weighed with a precision of 1 mg and placed in a sterile tube with a lid, and 1 mL distilled water was added to each one. The mixtures were diluted fivefold and sonicated in an ultrasonic bath for 20 min to prevent potential agglomeration. A small drop of each dispersion solution was spread onto an FE-SEM slide, and the slide was gold–palladium sputter-coated (Quorum Q150R ES, Quorum Technologies Ltd, Lewes, UK). The imaging process was operated at 30 kV, and the images were taken with 50.00 KX magnifications.

2.5 Anticancer activities of SnO_2 and TiO_2 nanoparticles

MCF-7 cells were cultivated in Dulbecco's Modified Eagle's Medium (DMEM, Sigma) supplemented with 10% fetal bovine serum (FBS, Biowest) and 1% penicillin/streptomycin mixture (Gibco) under 5% CO_2 in a humidified environment at 37 °C, as previously reported [45]. The cultivated cells were introduced in 96-well plates (Corning, Costar) in 100 µL, with a density of 1×10^4 cells per well, and left for 24 h of incubation. Next, the cells were exposed to varying concentrations (0–1000 ppm) of the synthesized nanoparticles for 24 h. The viability of the cells after treatment periods was determined using the MTT (3-(4,5-dimethylthiazol-2-yl)−2,5-diphenyltetrazoliumbromid) test, as previously reported [46]. Briefly, 25 µL of 5 mg/mL MTT solutions was added to each well and incubated at 37 °C for 4 h. Eventually, the resulting formazan crystals were dissolved in 100 µL of DMSO, and color was measured with a wavelength of 590 nm using a microplate spectrophotometer. Cell viability was expressed as percentage survival, with 100% survival taken as that observed in the untreated control (cell culture control). All the experiments were carried out in triplicate, and the data are reported as the mean of cell proliferation percentage ± SD. The differences in variance were analyzed statistically using a one-way analysis of variance (ANOVA) test by GraphPad Prism version 8.4.2 (GraphPad Software Inc.; La Jolla, CA).

2.6 Antifungal activities of SnO_2 and TiO_2 nanoparticles

The antifungal effects of SnO_2NPs and TiO_2NPs were evaluated against four different strains of *S. cerevisiae* BY4741 cells (wild type and its isogenic deletion mutants for cytosolic catalase T (ΔCTT1), thioredoxin-disulfide reductase (ΔTRR2), and glutathione synthase (ΔGSH2)) as well as *C. albicans* 64548. The routine maintenance of all the yeast cells was carried out on agar plates prepared with YPDA medium (10 g/L yeast extract, 20 g/L peptone, 20 g/L glucose, and 20 g/L Bacto agar, pH: 5.6) at 30 °C for 5 days. For the cytotoxicity assay, the cells were grown in YPD medium (10 g/L yeast extract, 20 g/L peptone, and 20 g/L glucose, pH: 5.6) at 30 °C until their mid-exponential phase. Geneticin was also added (200 mg/L) to the growth medium of mutant strains. Then, the cells at an initial concentration of 3×10^7 CFU/ml were treated with NPs at the concentration range of 0–400 ppm for 24 h with gentle shaking at 30 °C. At the end of incubation, OD values of the samples were measured at 660 nm against related blanks. The results were expressed as a percentage of proliferation compared with the untreated control group. All the experiments were carried

out in triplicate, and the data are reported as the mean of cell proliferation percentage ± SD. The differences in variance were analyzed statistically using a one-way analysis of variance (ANOVA) test by GraphPad Prism version 8.4.2 (GraphPad Software Inc.; La Jolla, CA).

3 Results and discussion

3.1 Synthesis of SnO_2 and TiO_2 nanoparticles

The general plant-based synthesis procedure for preparing NPs basically consists of three main steps, including preparation of clear plant extract, mixing with appropriate precursor, and finally calcification or dehydration at high temperatures [47]. In this study, water extracts of the nutritional plants *Cnicus benedictus* and *Aronia melanocarpa* were utilized as precursors and capping agents to synthesize SnO_2NPs and TiO_2NPs, respectively. In the green synthesis procedure of the SnO_2NPs, briefly, the biomolecules in the plant extract, including polyphenols, flavonoids, and other antioxidants, facilitate the oxidation of the Sn^{2+} ions in the salt solution to the Sn^{4+}. The Sn^{4+} ions undergo hydrolysis to produce tin hydroxide ($Sn(OH)_4$), which subsequently undergoes condensation to form SnO_2NPs. In a similar manner, the titanium hydroxide ($Ti(OH)_4$), which is produced by the hydrolysis of the $[Ti(OCH(CH_3)_2]_4$, undergoes a condensation reaction, resulting in the formation of TiO_2NPs. At the end, the formed NPs are stabilized with bioactive molecules in the plant extract [48, 49].

3.2 Spectroscopic and microscopic characterization of SnO_2 and TiO_2 nanoparticles

XRD analysis is one of the most important methods used in the characterization of nanoparticle structure [50]. This method enables the determination of the structure, components, and particle size of the sample. When the particle size drops below 100 nm, a diffraction line occurs [51]. The XRD diffraction patterns of SnO_2NPs and TiO2NPs are given in Fig. 1A and B, respectively. As evident from the diffraction patterns, SnO_2NPs were successfully produced with a tetragonal crystal structure and lattice parameters $a = 4.737$ Å and $c = 3.186$ Å. The average particle size of the nanoparticles calculated according to the Debye–Scherrer formula was found to be approximately 27.48 nm. It was determined that the most intense peaks of the SnO_2NPs belonged to the (110), (101), (200), (211), (220), (310), and (311) directions,

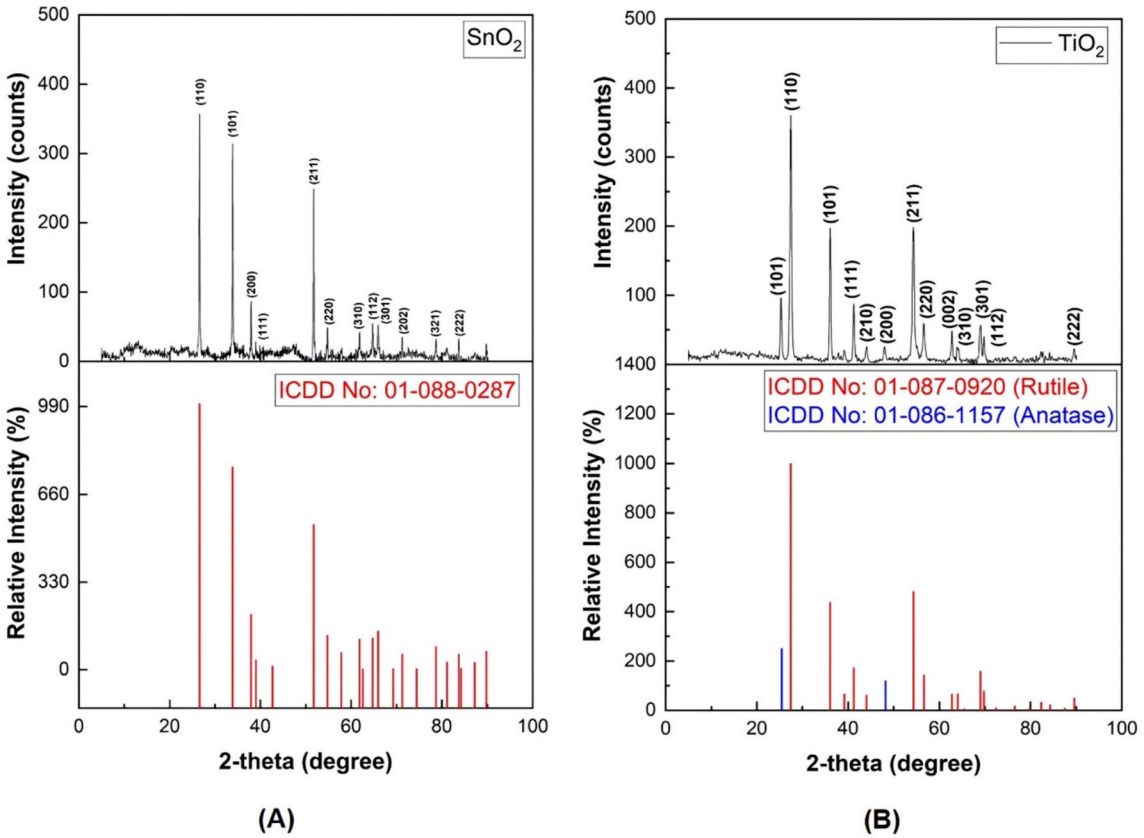

Fig. 1 XRD patterns of **A** SnO_2NPs synthesized using *Cnicus benedictus* extract and **B** TiO_2NPs synthesized using *Aronia melanocarpa* extract

which were observed at 2Θ = 26.73°, 34.13°, 37.8°, 51.7°, 54.85, 62.01°, and 66,2° (Fig. 1A). These results were in full compliance with JCPDS card number 01–088–0287 and were also in perfect harmony with the study of Kumar et al. (2018) [38]. The XRD examination results indicated that the peaks observed in the TiO_2NPs were oriented towards the rutile and anatase phases. The composition of the structure consists of roughly 80% rutile and 20% anatase. According to the ICDD library (ICDD card no. 01–087–0920), the dominant rutile phase in the structure has a tetragonal structure with lattice parameters of $a = 5.594$ and $c = 2.958$. The average particle size of the rutile phase calculated according to the Debye–Scherrer formula is approximately 19.88 nm. In Fig. 1B, the X-ray diffractogram of the TiO_2NPs sample is given together with Miller indices (orientation planes). In the spectrum obtained from the reflections of nanoparticles diffracted between 5° and 90° at 2Θ angle, sharp peaks were seen at 27°, 36°, 41°, 54°, 56 °, and 69°. These peaks match (110), (101), (111), (211), (220), and (301) directions, respectively. The peak seen at 27° is completely identical to the rutile structure of TiO_2NPs [51]. The peaks detected at 2Θ = 24.8°, 48.7°, and 39° are distinctive peaks that indicate the presence of TiO_2NPs in the anatase structure [52].

Figure 2A shows the ATR-FTIR spectra of the SnO_2NPs and *Cnicus benedictus* extract. The peak at 3212 cm^{-1} displayed the possible presence of H-bonding between OH functional groups and N–H stretching originating from alcohol and/or phenols in the plant extract. In the ATR-FTIR analysis of SnO_2NPs, the 2973 cm^{-1} peak is the reciprocal of the C-H stretching vibration. The ATR-FTIR chromatogram of the plant extract showed peaks at 1586 cm^{-1}, 1292 cm^{-1}, and 1041 cm^{-1}, which can be attributed to the stretching vibrations of C = C and C-O bonds typically found in aromatic rings and alcohols of flavonoids and phenolic

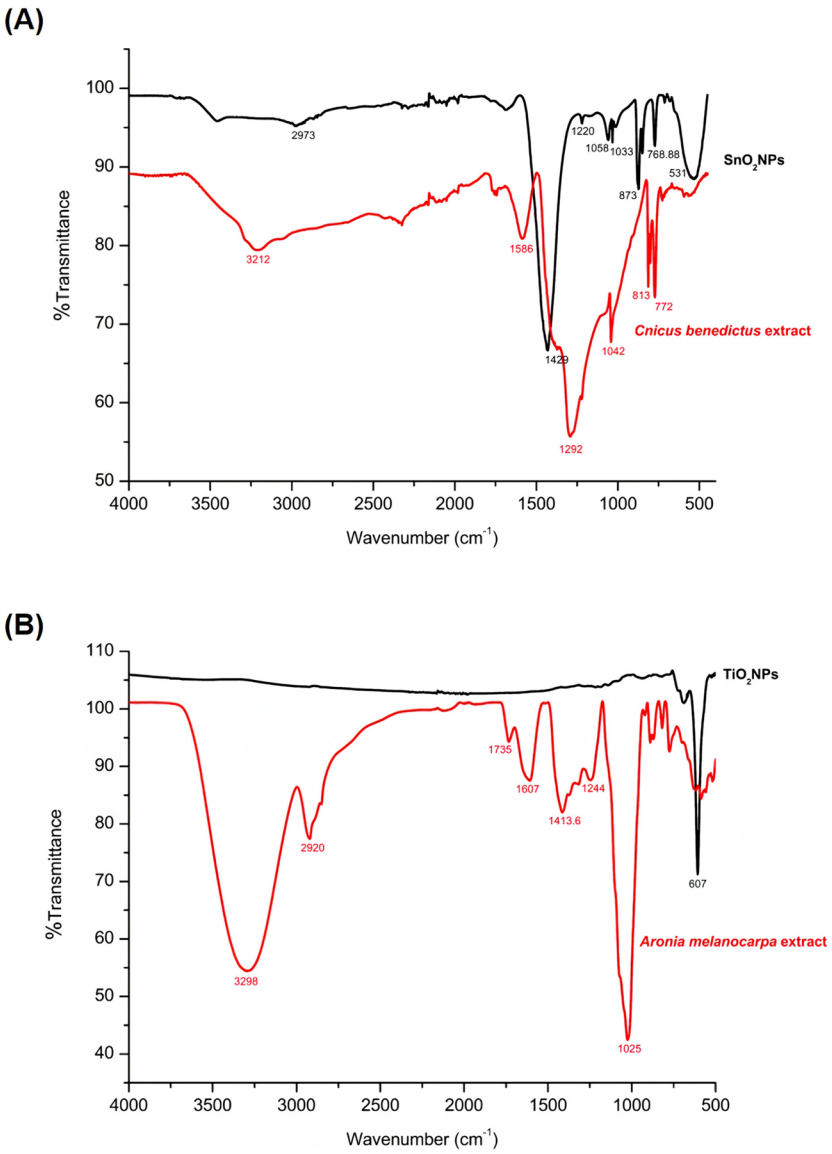

Fig. 2 Attenuated total reflection-Fourier transform infrared spectra of SnO_2NPs and *Cnicus benedictus* extract (**A**) and TiO_2NPs and *Aronia melanocarpa* extract (**B**)

acids, respectively [53, 54]. The observation of much weaker peaks at around the same locations in the chromatogram of SnO_2NPs may indicate the presence of the coating agent. The peaks located at 1429 cm^{-1} and 1058 cm^{-1} in the FTIR spectra of SnO_2NPs showed the presence of C = C and C-O stretching as well as asymmetric and symmetrical stretching of the carboxylate group. The most obvious difference between the two spectra was the 530 cm^{-1} peak of SnO_2NPs. This peak shows the presence of a metal–oxygen bond, and it is the characteristic vibration peak of the O–Sn–O bond [55, 56]. Figure 2B illustrates the ATR-FTIR spectra of the TiO_2NPs, and the *Aronia melanocarpa* extract. *Aronia* fruit showed absorption frequencies at 2920 cm^{-1}, 1607 cm^{-1}, and 1025–1244 cm^{-1}, corresponding to C-H, C–C, and C-O stretching modes, respectively. Additionally, the absorption at 1413.6 cm^{-1} was attributed to the C-H originating from cyclic structures and the O–H bending vibrations from alcohols and carboxylic acids. The peaks occurring after 600 cm^{-1} in the ATR-FTIR spectrum of TiO_2NPs were due to Ti–O stretching vibration [57].

The FE-SEM images of SnO_2NPs and TiO_2NPs can be visualized in Fig. 3A and B, respectively. It was determined that the obtained SnO_2NPs had a spherical structure with the particle size in the range of 24–29 nm [58]. On the other hand, morphological characterization of TiO_2NPs showed that it was not distributed homogeneously, and there were clustered particles in the structure due to the unstable structure of these nanoparticles [59]. The TiO_2NPs exhibited diameters ranging from 60 to 90 nm. Actually, to address this issue, the nanoparticles were carefully stored in a vacuum desiccator following synthesis to reduce agglomeration. Prior to their use in further experiments or characterization, they were subjected to ultrasonic dispersion to improve their stability. Furthermore, approaches such as surface modification (e.g., coating with polymers or organic ligands), optimization of synthesis parameters (e.g., pH control or the use of stabilizing agents), or the inclusion of dispersing agents could offer additional means to mitigate stability challenges. These strategies, which are well-established for enhancing nanoparticle dispersity, will be explored in subsequent research.

EDX spectra of SnO_2NPs and TiO_2NPs were presented in Fig. 3C and D, respectively. The presence of Sn and O was clearly observed in the EDX spectrum of the SnO_2NPs, and the percentages of these elements were determined as 51.45% and 37.01%, respectively, which confirmed the formation of SnO_2. The EDX results also showed the presence of the other elements, which most likely originating from

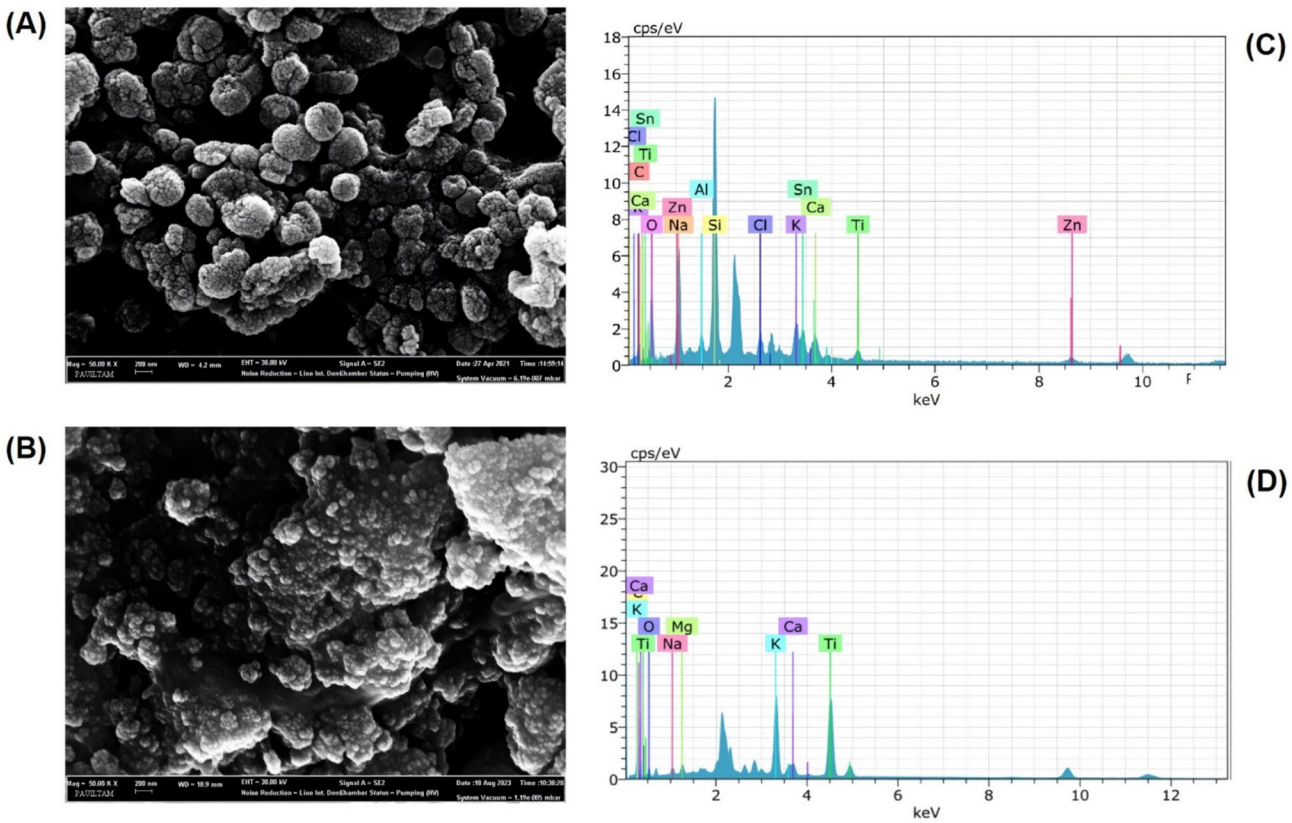

Fig. 3 FE-SEM images and EDX spectra of SnO_2NPs synthesized using *Cnicus benedictus* extract (**A**, **C**) and TiO_2NPs synthesized using *Aronia melanocarpa* extract (**B**, **D**)

the *Cnicus benedictus* extract. While the Al element (0.52%) in the spectrum arose from aluminum foil during sample processing, Cl (3.28%) was due to the precursor. The EDX spectrum of TiO_2NPs clearly confirmed the presence of titanium, with an elemental composition of 48%. In addition, the strong signal at 4.2 keV unequivocally confirms that the major component is Ti [60]. Finally, the distinct oxygen (O), calcium (Ca), potassium (K), magnesium (Mg), and nitrogen (N) signals were detected mostly because of plant extract.

3.3 Anticancer activities of SnO_2 and TiO_2 nanoparticles against human breast cancer cell line

The anticancer activities of the SnO_2NPs and TiO_2NPs at the concentration range of 25–1000 ppm was studied against the MCF-7 cell line by MTT assay (Fig. 4). The findings demonstrated a positive correlation between the concentration of nanoparticles and their antiproliferative effects, mostly in a statistically significant manner. At a concentration of 100 ppm, the SnO_2NPs and TiO_2NPs decreased cell viability to 56.09% and 62.88%, respectively. Nevertheless, it is important to mention that there were no dramatic reductions in cell proliferation as the concentrations of the nanoparticles were elevated to higher levels. The highest concentration of the SnO_2NPs and TiO_2NPs decreased cell viability to 43.45% and 49.66%, respectively. Consistent with our findings, a study revealed that a concentration of 93.55 µg/mL of SnO_2NPs, which were synthesized using an extract from *Matricaria recutita* leaves, resulted in a 50% reduction in the growth of human melanoma cells [61]. Similarly, Manimaran et al. (2024) reported that *Hypsizygus ulmarius*-mediated TiO_2NPs inhibited the proliferation of the liver cancer cell line by 50% at 83.3 µg/mL [62]. Most

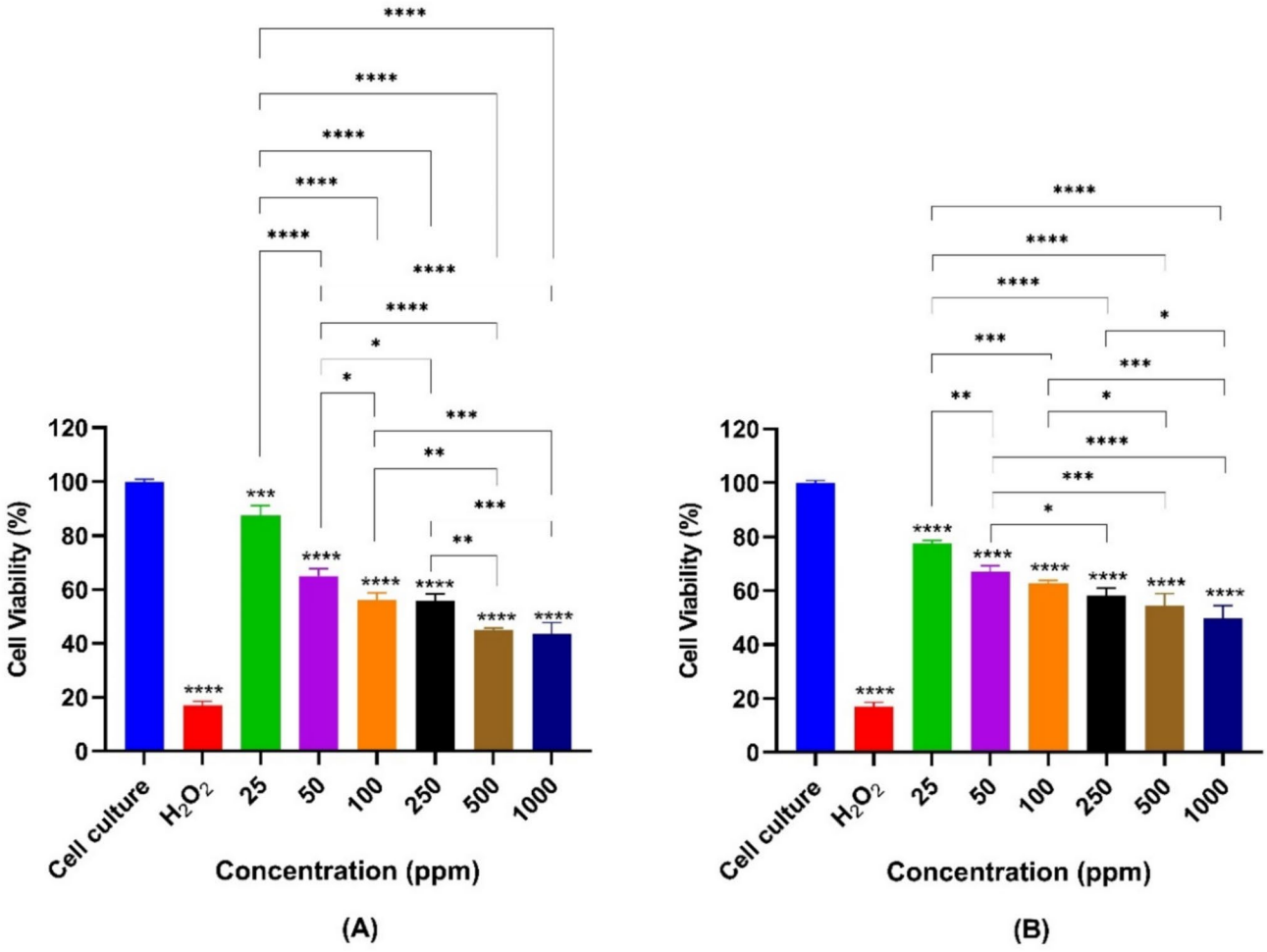

Fig. 4 Anticancer effects of SnO_2NPs and TiO_2NPs at the concentration range of 0–1000 ppm. Cell viability (%) was measured after 24-h treatment with the NPs. Data are presented as mean ± SD of three independent experiments. *$p < 0.05$; **$p < 0.01$; ***$p < 0.001$; ****$p < 0.0001$ denote significant differences between control and other studied group or indicated groups by Tukey's multiple range tests

chemotherapeutic and anticancer drugs demonstrate efficacy in in vitro cell culture experiments at concentrations between 0.1 and 10 ppm, indicating that although the findings are encouraging, the doses reported in this study are comparatively elevated relative to those documented in the literature.

Reviewing the literature suggests that intracellular reactive oxygen species (ROS) generation underlies the cytotoxicity mechanisms of SnO_2NPs. Key findings from research showed that SnO_2NPs induced cytotoxicity, cell cycle arrest, and a reduction in mitochondrial membrane potential in MCF-7 cells in a dose- and time-dependent manner. The study also demonstrated that SnO_2NPs disrupted redox homeostasis by depleting antioxidants such as glutathione, superoxide dismutase, and catalase and increasing oxidant levels. Furthermore, the antioxidant N-acetyl cysteine effectively reduced the cytotoxicity, GSH depletion, and ROS generation that were induced by SnO_2NPs [63]. All these results emphasize the significance of oxidative stress in the cytotoxicity induced by SnO_2NPs. On the other hand, TiO_2NPs appear to exhibit anticancer potential through multiple mechanisms including suppression of cell migration and colony formation, upregulation of tumor suppressor genes such as tumor protein p53, melanoma differentiation-associated protein 7 (MDA7), tumor necrosis factor-related apoptosis-inducing ligand (TRAIL), and the signal transducer and activator of transcription 3 (STAT3) [64]. Moreover, TiO_2NPs have been reported to produce ROS [65], albeit at low levels, which may nonetheless be sufficient to induce cell death in cancer cells with an already weakened antioxidant defense system. However, it is important to note that these effects may vary depending on the physical properties of the synthesized nanoparticles, highlighting the need for further investigation.

3.4 Antifungal activities of SnO_2 and TiO_2 nanoparticles against Saccharomyces cerevisiae and *Candida albicans* strains

In this paper, the antimicrobial activities of the green synthesized SnO_2NPs from *Cnicus benedictus* extract and TiO_2NPs from *Aronia melanocarpa* extract were investigated against four different *S. cerevisiae* strains, namely wild-type *S. cerevisiae* BY4741 and ΔCTT1, ΔTRR2, and ΔGSH2 mutants, besides *C. albicans*. As is well known, *C. albicans* is one of the most prevalent fungal pathogens, capable of causing a wide range of infections that vary in severity from superficial to systemic. Superficial infections, such as cutaneous candidiasis, commonly affect warm, moist, and creased areas of the skin, while mucosal sites like the oral cavity and vagina are also frequently impacted [66]. In more severe cases, *C. albicans* can invade deeper tissues, leading to systemic infections such as candidemia or invasive candidiasis, which can affect vital organs like the liver, kidneys, and brain, particularly in immunocompromised individuals. This wide spectrum of infections highlights the opportunistic nature of *C. albicans* and its capacity to adapt to diverse host environments. In a similar vein, *S. cerevisiae*, a unicellular eukaryotic yeast, exhibits dual roles as a beneficial microorganism and a potential health risk. As its name suggests, this yeast is a critically important microorganism in the production of many food and alcoholic beverages [67]. On the other hand, it is also accepted as the organism responsible for food spoilage [68]. Besides, there are cases where it has negative effects on human health. It has been reported that the use of *S. cerevisiae* probiotics should be carefully reassessed, particularly in immunosuppressed or critically ill patients [69, 70]. Due to all the aforementioned reasons, it is quite significant to be able to control the proliferation of this yeast species. The mutant strains were used to examine the potential protective effects of the corresponding antioxidant enzymes, catalase (CAT), thioredoxin reductase (Trx), and glutathione synthase (GS), which are produced by these deleted genes, respectively. Briefly, it is known for a long time that yeast CATs have an important role in removal of H_2O_2, especially during stationary phase, and may play some part in the adaptive response to oxidative stress [71]. Trx regulates the intracellular redox environment by reducing thioredoxin, and finally, GS is responsible for the synthesis of glutathione (GSH), which is the most abundant non-protein thiol that protects cells from oxidative damage and the toxicity of xenobiotic electrophiles and maintains redox homeostasis [72].

The results were presented in Figs. 5 and 6. As shown in Fig. 5, 200–400 ppm was determined as the effective dose range of the green synthesized SnO_2NPs against wild-type *S. cerevisiae*, which suggests that the wild strain is resistant to relatively low doses of SnO_2NPs (Fig. 5A). Despite the fact that TiO_2NPs exhibited statistically significant reductions in cell proliferation at concentrations of 200 and 400 ppm in comparison to the control ($p < 0.0001$), no significant antimicrobial activity was observed even at the highest concentration examined (Fig. 5B). This limited activity may be attributed to the predominant rutile crystal phase in TiO_2NPs, which has a narrower band gap compared to the anatase phase. The narrower band gap can result in reduced photocatalytic activity and lower generation of ROS, which are critical for antimicrobial effects. A finding supporting our result was put forward by Kasemets et al. (2009), who stated that the IC_{50} value of TiO_2NPs against yeast cells was over 20,000 ppm [73]. In contrast, SnO_2NPs demonstrated promising antifungal activity, potentially due to their wide band gap, which facilitates the generation of ROS [63]. This activity can also be linked to the tetragonal crystal structure of SnO_2NPs, with lattice parameters of $a = 4.737$ Å and $c = 3.186$ Å. The precise arrangement of atoms in the tetragonal structure could enhance surface reactivity and

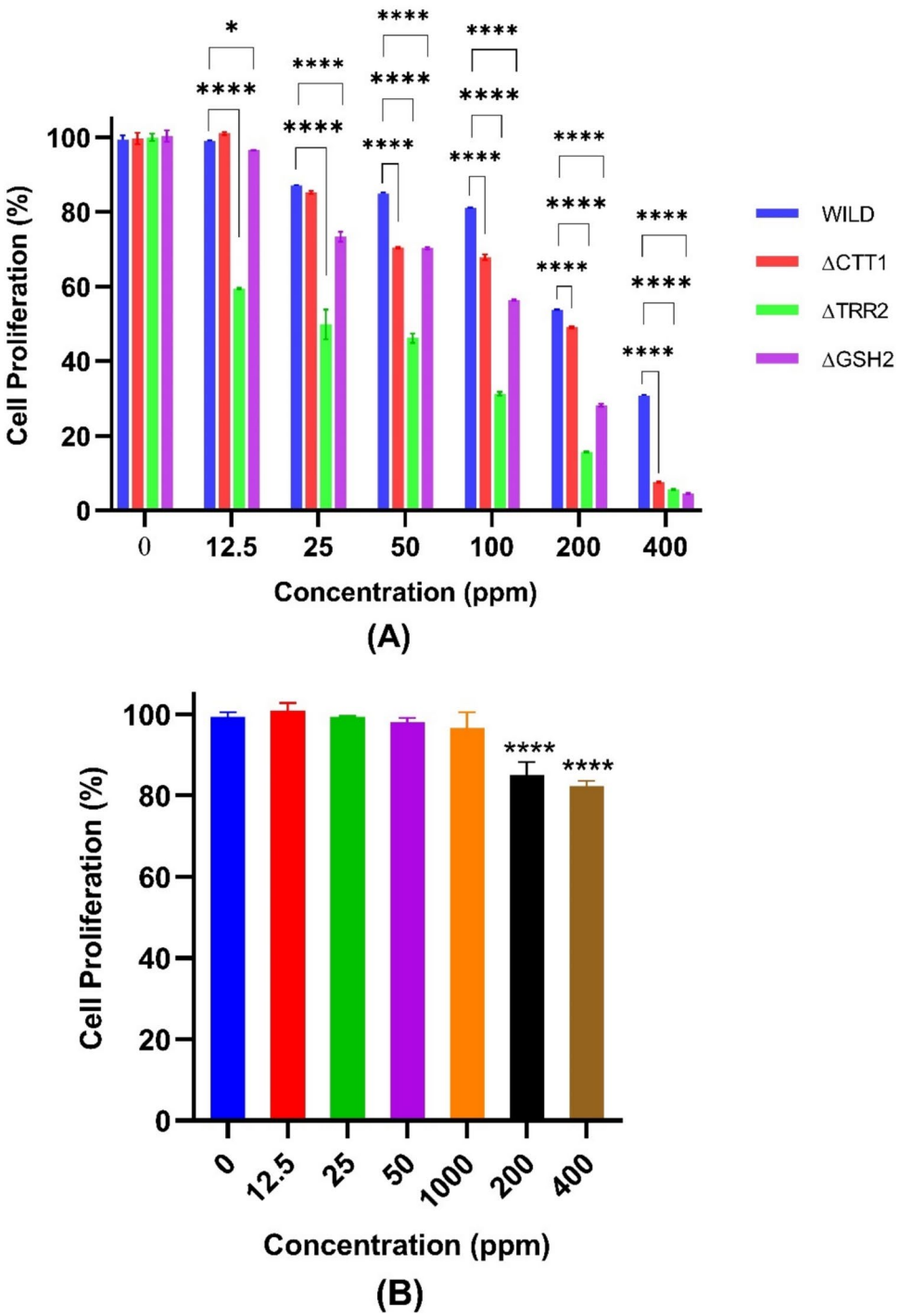

Fig. 5 Antifungal activities of SnO_2NPs (**A**) and TiO_2NPs (**B**) at the concentration range of 0–400 ppm against *S. cerevisiae*. Cell proliferation (%) was measured after 24-h treatment with the NPs. Data are presented as mean ± SD of three independent experiments. $^*p < 0.05$; $^{****}p < 0.0001$ denote significant differences between control and other studied group or indicated groups by Tukey's multiple range tests

electron transfer processes, contributing to efficient ROS generation. Therefore, the investigation of mutant strains was limited to SnO_2NPs. As anticipated, all mutant yeast strains exhibited greater sensitivity to SnO_2NPs compared to the wild-type strain at almost all studied concentrations. IC_{50} values of the SnO_2NPs were calculated as 131.7, 126.8, 86.63, and 78.86 ppm on wild, ΔCTT1, ΔGSH2, and ΔTRR2 mutants, respectively. These results showed that especially the TRR2 and GSH2 deletions made the organism much more susceptible to SnO_2NPs treatment. Thus, it is regarded that the level of reactive species increases with the treatment of SnO_2NPs and destroys the redox state of yeast cells. Consistent with these findings, previous studies have demonstrated intracellular ROS generation by SnO_2NPs at 100 ppm without inducing significant toxicity in wild type *S. cerevisiae* cells [74]. Additionally, in a current study conducted on two different bacterial strains, the antimicrobial activity of the biosynthetic SnO_2NPs was based on

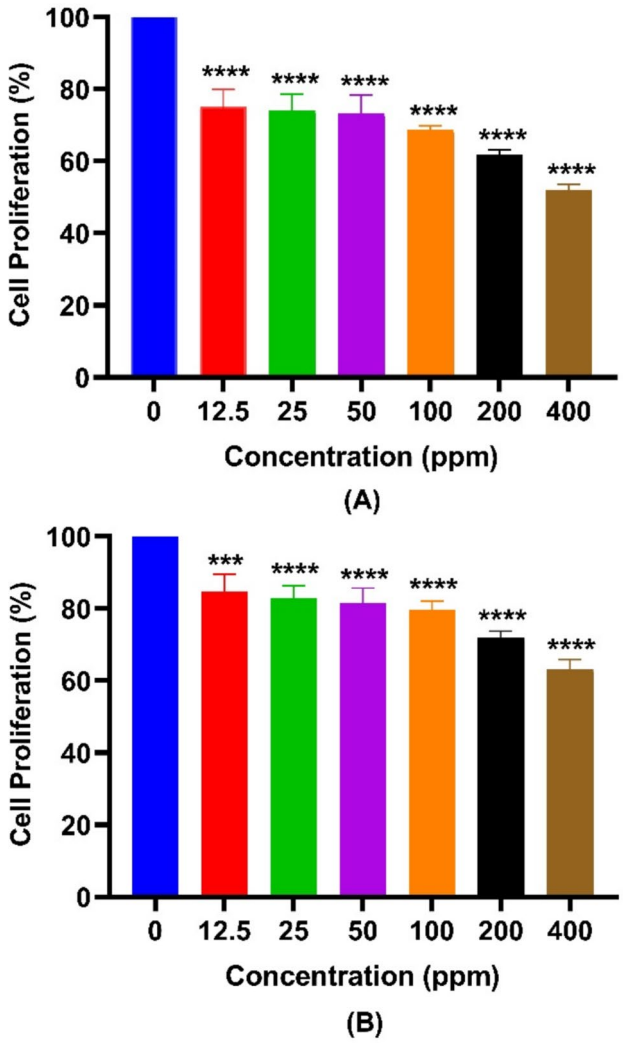

Fig. 6 Antifungal activities of SnO_2NPs (**A**) and TiO_2NPs (**B**) at the concentration range of 0–400 ppm against *C. albicans*. Cell proliferation (%) was measured after 24-h treatment with the NPs. Data are presented as mean ± SD of three independent experiments. ***$p < 0.001$; ****$p < 0.0001$ denote significant differences between control and other studied group or indicated groups by Tukey's multiple range tests

stimulated ROS production [75]. Figure 6 presents the antifungal effects of SnO_2NPs and TiO_2NPs against *C. albicans* cells. The synthesized nanoparticles were observed to be efficacious against *C. albicans* cells only at high concentrations, as was the case with *S. cerevisiae* cells. At the highest concentration tested, 400 ppm, the viability of *C. albicans* cells treated with SnO_2NPs was 52.09 ± 1.42%, while the viability of those treated with TiO_2NPs was 61.74 ± 1.43%. It is evident that SnO_2NPs are more effective on *C. albicans* cells as well. Previous studies have reported that biocompatible SnO_2NPs exhibited antifungal activity against *C. albicans*, with a minimum inhibitory concentration (MIC) of 8 mg/mL and a minimum fungicidal concentration (MFC) of > 16 mg/mL. Finally, although there is no evidence of the toxic effects of SnO_2NPs specifically against *S. cerevisiae*, it has been found that these nanoparticles have antiproliferative effects on various other microorganisms at a wide concentration range from 0.03 ppb to 1000 ppm [76, 77].

4 Conclusion

The ecological synthesis of NPs has become increasingly important in recent years as a result of its diverse range of applications in both economic and environmental sectors. In contrast to conventional chemical synthesis, green methods provide an environmentally friendly alternative by reducing the use of toxic chemicals and utilizing natural resources, thereby aligning with global sustainability objectives. The green nanoparticle synthesis process has been appealing to both researchers and industries due to its economic viability and environmental advantages, which provide a flexible and versatile platform for a variety of applications. This study presents the production and characterization of SnO_2 and TiO_2 NPs from *Cnicus benedictus* and *Aronia melanocarpa* extracts using a green synthesis process, respectively. The presence of green synthesized NPs was verified by the characterization methods, which included XRD, FTIR, and SEM–EDX. Although both NPs demonstrated favorable anticancer effects on MCF-7 cells, only the SnO_2NPs exhibited significant antifungal effects on all of the yeast strains that were tested. The most susceptible mutants were ΔTRR2 and ΔGSH2, primarily due to the mechanism of action, which is based on the production of ROS. These findings of the present study reflect the possible uses of biosynthesized SnO_2 and TiO_2 NPs in industries and clinics. For instance, the SnO_2NPs could have applications in antifungal therapies, specifically against resistant fungal species, and similarly, TiO_2NPs as candidates might have applications in anticancer treatments and environmental remediation. Besides, green synthesis of NPs, in comparison with conventional methods, provides competitiveness by means of sustainability due to cost reduction and diminishment of environmental impacts. However, the study also has certain limitations that warrant further exploration. The scalability of the green synthesis method remains a challenge, as its feasibility for large-scale production needs to be critically evaluated. Additionally, the biological relevance of the current findings should be further validated in more complex systems, such as in vivo models, to better understand the clinical and industrial applicability of these NPs. Moving forward, addressing these challenges could enhance the practical significance of green-synthesized SnO_2 and TiO_2 NPs, paving the way for their integration into sustainable technologies across biomedicine, environmental remediation, and material sciences.

Acknowledgements We would like to express our thanks to Dr. Duygu Takanoğlu Bulut and Nilüfer Aydınlık from Advanced Technology Application and Research Center of Pamukkale University (ILTAM) for SEM/EDX and XRD analyses.

Author contribution Mine Sulak and Berna Kavakcıoğlu Yardımcı: Writing, original draft; writing, review and editing; validation; investigation; formal analysis; methodology; data curation; resources.

Funding Open access funding provided by the Scientific and Technological Research Council of Türkiye (TÜBİTAK).

Data availability The data that support the findings of this study are available on request from the corresponding author. The data are not publicly available due to privacy or ethical restrictions.

Declarations

Ethics approval and consent to participate Not applicable.

Consent for publication Not applicable.

Competing interests The authors declare no competing interests.

References

1. Auffan M, Rose J, Bottero JY et al (2009) Towards a definition of inorganic nanoparticles from an environmental, health and safety perspective. Nat Nanotechnol 4:634–641
2. Frewer LJ, Gupta N, George S et al (2014) Consumer attitudes towards nanotechnologies applied to food production. Trends Food Sci Technol 40:211–225. https://doi.org/10.1016/j.tifs.2014.06.005
3. Charinpanitkul T, Faungnawakij K, Tanthapanichakoon W (2008) Review of recent research on nanoparticle production in Thailand. Adv Powder Technol 19:443–457. https://doi.org/10.1163/156855208X336693
4. Rad AG, Abbasi H, Afzali MH (2011) Gold nanoparticles: synthesising, characterizing and reviewing novel application in recent years. In: Physics Procedia. Elsevier B.V., pp 203–208
5. Das Purkayastha M, Manhar AK (2016) Nanotechnological applications in food packaging, sensors and bioactive delivery systems. pp 59–128
6. Mittal AK, Chisti Y, Banerjee UC (2013) Synthesis of metallic nanoparticles using plant extracts. Biotechnol Adv 31:346–356
7. Kumari SC, Dhand V, Padma PN (2021) Green synthesis of metallic nanoparticles: a review. In: Praveen Kumar R, Bharathiraja B (eds) Nanomaterials. Academic Press, pp 259–281
8. Parveen K, BV, LL (2016) Green synthesis of nanoparticles: their advantages and disadvantages. In: AIP. AIP Publishing
9. Kaabipour S, Hemmati S (2021) A review on the green and sustainable synthesis of silver nanoparticles and one-dimensional silver nanostructures. Beilstein J Nanotechnol 12:102–136. https://doi.org/10.3762/BJNANO.12.9
10. Naseem K, Aziz A, Tahir MH et al (2024) Biogenic synthesized nanocatalysts and their potential for the treatment of toxic pollutants: environmental remediation, a review. Int J Environ Sci Technol 21:2163–2194
11. Jadoun S, Arif R, Jangid NK, Meena RK (2021) Green synthesis of nanoparticles using plant extracts: a review. Environ Chem Lett 19:355–374
12. Idris DS, Roy A (2023) Synthesis of bimetallic nanoparticles and applications—an updated review. Crystals (Basel) 13:637
13 Singh J, Dutta T, Kim KH et al (2018) "Green" synthesis of metals and their oxide nanoparticles: applications for environmental remediation. J Nanobiotechnology 16:1–24
14. Behera A, Patra N, Mittu B et al (2020) Bimetallic nanoparticles: green synthesis, applications, and future perspectives. In: Multifunctional Hybrid Nanomaterials for Sustainable Agri-food and Ecosystems. Elsevier, pp 639–682
15. El SAM (2020) Green synthesis of metal and metal oxide nanoparticles from plant leaf extracts and their applications: a review. Green Process Synthesis 9:304–339
16 Ziętal K, Mirowska-Guzel D, Nowaczyk A, Blecharz-Klin K (2024) Cnicus benedictus: folk medicinal uses, biological activities, and in silico screening of main phytochemical constituents. Planta Med 90:976–991
17. Piras A, Porcedda S, Smeriglio A, et al (2024) Chemical composition, nutritional, and biological properties of extracts obtained with different techniques from Aronia melanocarpa berries. Molecules 29. https://doi.org/10.3390/molecules29112577
18. Dülger D (2012) Cnicus benedictus'ün besleyici ve kimyasal özellikleri. Master's Thesis, Graduate School of Natural and Applied Sciences, Uludağ University, Bursa
19. Polat M, Mertoglu K, Eskimez I, Okatan V (2020) Effects of the fruiting period and growing seasons on market quality in goji berry (Lycium barbarum L.). Folia Horticulturae 32:229–239. https://doi.org/10.2478/fhort-2020-0021
20. Polat M, Guclu SF, Okatan V, Ercisli S, Ozaydin A, Colak AM, Askin MA (2017) Determination of phenolic compounds in aronia genotypes grown in Turkey. Oxid Commun 40(1-I):131–137
21. Gebreslassie YT, Gebretnsae HG (2021) Green and cost-effective synthesis of tin oxide nanoparticles: a review on the synthesis methodologies, mechanism of formation, and their potential applications. Nanoscale research letters 16(1):97. https://doi.org/10.1186/s11671-021-03555-6
22. Srivastava NMM (2014) Biosynthesis of SnO2 nanoparticles using bacterium Erwinia herbicola and their photocatalytic activity for degradation of dyes. Ind Eng Chem Res 53:13971–13979
23. Wang J, Wu W, Wang WH, Bao M (2017) Expeditious synthesis of SnO2 nanoparticles through controlled hydrolysis and condensation of tin alkoxide in reverse microemulsion. Ceram Int 43:4702–4705. https://doi.org/10.1016/j.ceramint.2017.01.002
24. Thamaphat K, Limsuwan P, Ngotawornchai B (2008) Phase characterization of TiO2 powder by XRD and TEM. Agric Nat Resour 42(5):357–361
25. Sadeghi Neisiani Z, Khaje M, Eslami Majd A (2023) Experimental comparison between Nb2O5- and TiO2-based photoconductive and photogating GFET UV detector. Sci Rep 13. https://doi.org/10.1038/s41598-023-34295-5
26. Bersch JD, Flores-Colen I, Masuero AB, Dal Molin DC (2023) Photocatalytic TiO2 based coatings for mortars on facades: a review of efficiency, durability, and sustainability. Buildings 13(1):186. https://doi.org/10.3390/buildings13010186

27. Oruç P, Turan N, Cavdar S et al (2023) Investigation of dielectric properties of amorphous, anatase, and rutile TiO2 structures. J Mater Sci: Materials in Electronics 34. https://doi.org/10.1007/s10854-023-09924-4
28. Sadeghpour H, Shafaei SZ, Ardejani FD et al (2023) Arsenic removal by highly efficient MnFe2O4/TiO2/g-C3N4 and MnFe2O4/TiO2/GO adsorbents from a groundwater sample, Bardsir, Iran. Environ Nanotechnol Monit Manag 20. https://doi.org/10.1016/j.enmm.2023.100821
29. Navidpour AH, Abbasi S, Li D, Mojiri A, Zhou JL (2023) Investigation of advanced oxidation process in the presence of TiO2 semiconductor as photocatalyst: property, principle, kinetic analysis, and photocatalytic activity. Catalysts 13(2):232. https://doi.org/10.3390/catal13020232
30. Heydari V, Abdouss M, Tajiki A, Pourmadadi M (2024) Influence of metal and nonmetal doping on wetting and dispersing characteristics of TiO2 pigment for coating applications. Prog Org Coat 188. https://doi.org/10.1016/j.porgcoat.2024.108211
31. Dülger B, Özkan G, Angı OS, Özkan G (2024) Green synthesis of TiO2 nanoparticles using aloe vera extract as catalyst support material and studies of their catalytic activity in dehydrogenation of Ethylenediamine Bisborane. Int J Hydrogen Energy 75:466–474. https://doi.org/10.1016/j.ijhydene.2024.02.223
32. Rajaram P, Jeice AR, Jayakumar K (2023) Review of green synthesized TiO2 nanoparticles for diverse applications. Surf Interfaces 39:102912
33. Rathi VH, Jeice AR (2023) Green fabrication of titanium dioxide nanoparticles and their applications in photocatalytic dye degradation and microbial activities. Chemical Physics Impact 6. https://doi.org/10.1016/j.chphi.2023.100197
34. Mohammed HA, Eddine LS, Souhaila M et al (2024) Green synthesis of SnO2 nanoparticles from Laurus nobilis L. extract for enhanced gelatin-based films and CEF@SnO2 for efficient antibacterial activity. Food Bioproc Tech 17:1364–1382. https://doi.org/10.1007/s11947-023-03209-8
35. Aliyu-Amoo H, Isa HI, Njoya EM, McGaw LJ (2021) Antiproliferative effect of extracts and fractions of the root of Terminalia avicennioides (Combretaceae) Guill and Perr. on HepG2 and Vero cell lines. Clin Phytoscience 7. https://doi.org/10.1186/s40816-021-00307-y
36. Gowri S V (2016) In vitro assessment of antioxidant and antibacterial activity of green synthesized silver nanoparticles from Digitaria radicosa leaves. 9:
37 Hong GB, Jiang C-J (2018) Biosynthesis of SnO2 nanoparticles based on response surface methodology and the study of their dye removal. J Nanosci Nanotechnol 18:5020–5025
38. Kumar I, Mondal M, Sakthivel N (2018) Green synthesis of phytogenic nanoparticles. In: Green Synthesis, Characterization and Applications of Nanoparticles. Elsevier, pp 37–73
39. Ahmad W, Jaiswal KK, Soni S (2020) Green synthesis of titanium dioxide (TiO2) nanoparticles by using Mentha arvensis leaves extract and its antimicrobial properties. Inorg Nano-Metal Chem 50:1032–1038. https://doi.org/10.1080/24701556.2020.1732419
40. Bunaciu AA, Udriştioiu E, gabriela, Aboul-Enein HY, (2015) X-ray diffraction: instrumentation and applications. Crit Rev Anal Chem 45:289–299
41. Monshi A, Foroughi MR, Monshi MR (2012) Modified Scherrer equation to estimate more accurately nano-crystallite size using XRD. World J Nano Sci Eng 02:154–160. https://doi.org/10.4236/wjnse.2012.23020
42. Selvakumari JC, Ahila M, Malligavathy M, Padiyan DP (2017) Structural, morphological, and optical properties of tin(IV) oxide nanoparticles synthesized using Camellia sinensis extract: a green approach. Int J Miner Metall Mater 24:1043–1051. https://doi.org/10.1007/s12613-017-1494-2
43. Frost MS, Dempsey MJ, Whitehead DE (2017) The response of citrate functionalised gold and silver nanoparticles to the addition of heavy metal ions. Colloids Surf A Physicochem Eng Asp 518:15–24
44. Newbury DE, Ritchie NWM (2013) Is scanning electron microscopy/energy dispersive X-ray spectrometry (SEM/EDS) quantitative? Scanning 35:141–168. https://doi.org/10.1002/sca.21041
45. Gürel CM, Bozbeyoğlu NN, Yardımcı BK et al (2024) Biosourced polymeric cryogels for future biomedical applications with remarkable antimicrobial activities and tribological properties. Mater Today Commun 38. https://doi.org/10.1016/j.mtcomm.2024.108387
46. Tarhan L, Nakipoğlu M, Kavakcıoğlu B et al (2016) The induction of growth inhibition and apoptosis in HeLa and MCF-7 cells by Teucrium sandrasicum, having effective antioxidant properties. Appl Biochem Biotechnol 178:1028–1041. https://doi.org/10.1007/s12010-015-1926-2
47. Matussin S, Harunsani MH, Tan AL, Khan MM (2020) Plant-extract-mediated SnO2 nanoparticles: synthesis and applications. ACS Sustain Chem Eng 8:3040–3054
48. Thakur S, Karak N (2012) Green reduction of graphene oxide by aqueous phytoextracts. Carbon N Y 50:5331–5339. https://doi.org/10.1016/j.carbon.2012.07.023
49. Issaabadi Z, Nasrollahzadeh M, Sajadi SM (2017) Green synthesis of the copper nanoparticles supported on bentonite and investigation of its catalytic activity. J Clean Prod 142:3584–3591. https://doi.org/10.1016/j.jclepro.2016.10.109
50. Mourdikoudis S, Pallares RM, Thanh NTK (2018) Characterization techniques for nanoparticles: comparison and complementarity upon studying nanoparticle properties. Nanoscale 10:12871–12934
51. Sunkar S, Nachiyar CV, Lerensha R, Renugadevi K (2014) Biogenesis of TiO2 nanoparticles using endophytic Bacillus cereus. J Nanoparticle Res 16. https://doi.org/10.1007/s11051-014-2681-y
52. Cui L, Hui KN, Hui KS et al (2012) Facile microwave-assisted hydrothermal synthesis of TiO 2 nanotubes. Mater Lett 75:175–178. https://doi.org/10.1016/j.matlet.2012.02.004
53. Oliveira RN, Mancini MC, de Oliveira FCS et al (2016) Análise por FTIR e quantificação de fenóis e flavonóides de cinco produtos naturais disponíveis comercialmente utilizados no tratamento de feridas. Revista Materia 21:767–779. https://doi.org/10.1590/S1517-707620160003.0072
54. Yao G, Ma Y, Muhammad M, Huang Q (2019) Understanding the infrared and Raman spectra of ganoderic acid A: an experimental and DFT study. Spectrochim Acta A Mol Biomol Spectrosc 210:372–380. https://doi.org/10.1016/j.saa.2018.11.019
55. Amalric-Popescu D, Bozon-Verduraz F (2001) Infrared studies on SnO 2 and Pd/SnO 2. Catal Today 70:139–154
56. Gomathi E, Jayapriya M, Arulmozhi M (2021) Environmental benign synthesis of tin oxide (SnO2) nanoparticles using Actinidia deliciosa (Kiwi) peel extract with enhanced catalytic properties. Inorg Chem Commun 130. https://doi.org/10.1016/j.inoche.2021.108670
57. Bagheri S, Shameli K, Abd Hamid SB (2013) Synthesis and characterization of anatase titanium dioxide nanoparticles using egg white solution via Sol-Gel method. J Chem. https://doi.org/10.1155/2013/848205
58. Awoke N, Pandey D, Habtemariam AB (2022) Synthesis of Tin(IV) Oxide nanoparticles using plant leaf extracts of Vernonia amygdalina and Mentha spicata. Regen Eng Transl Med 8:407–412. https://doi.org/10.1007/s40883-021-00218-x
59. Keklikcioğlu Çakmak N, Topal Canbaz G (2020) TiO2 Nanopartikülü ve TiO2/Aktif Çamur Sentezi ile Sulu Çözeltiden Cu (II) İyonlarının Adsorpsiyonu. Gümüşhane Üniversitesi Fen Bilimleri Enstitüsü Dergisi. https://doi.org/10.17714/gumusfenbil.514285

60. Vu THT, Au HT, Tran LT et al (2014) Synthesis of titanium dioxide nanotubes via one-step dynamic hydrothermal process. J Mater Sci 49:5617–5625. https://doi.org/10.1007/s10853-014-8274-4
61. Mini JJ, Khan S, Aravind M, et al (2024) Investigation of antimicrobial and anti-cancer activity of thermally sensitive SnO2 nanostructures with green-synthesized cauliflower morphology at ambient weather conditions. Environ Res 245. https://doi.org/10.1016/j.envres.2023.117878
62. Manimaran K, Loganathan S, Prakash DG, Natarajan D (2024) Antibacterial and anticancer potential of mycosynthesized titanium dioxide (TiO2) nanoparticles using Hypsizygus ulmarius. Biomass Convers Biorefin 14:13293–13301. https://doi.org/10.1007/s13399-022-03186-6
63. Ahamed M, Akhtar MJ, Majeed Khan MA, Alhadlaq HA (2018) Oxidative stress mediated cytotoxicity of tin (IV) oxide (SnO 2) nanoparticles in human breast cancer (MCF-7) cells. Colloids Surf B Biointerfaces 172:152–160. https://doi.org/10.1016/j.colsurfb.2018.08.040
64. SreeLatha T, Reddy MC, Muthukonda SV et al (2017) In vitro and in vivo evaluation of anti-cancer activity: shape-dependent properties of TiO2 nanostructures. Mater Sci Eng C 78:969–977. https://doi.org/10.1016/j.msec.2017.04.011
65. Shukla RK, Sharma V, Pandey AK et al (2011) ROS-mediated genotoxicity induced by titanium dioxide nanoparticles in human epidermal cells. Toxicol In Vitro 25:231–241. https://doi.org/10.1016/j.tiv.2010.11.008
66. Herculano RD, dos Reis CE, de Souza SMB et al (2024) Amphotericin B-loaded natural latex dressing for treating Candida albicans wound infections using Galleria mellonella model. J Control Release 365:744–758. https://doi.org/10.1016/j.jconrel.2023.12.010
67 Stewart GG (2016) Saccharomyces species in the production of beer. Beverages 2:34
68. Smits GJ, Brul S (2005) Stress tolerance in fungi - to kill a spoilage yeast. Curr Opin Biotechnol 16:225–230. https://doi.org/10.1016/j.copbio.2005.02.005
69. Riquelme AJ, Calvo MA, Guzmán AM, Depix MS, García P, Pérez C, Labarca JA (2003) Saccharomyces cerevisiae fungemia after Saccharomyces boulardii treatment in immunocompromised patients. J Clin Gastroenterol 36(1):41–43. https://doi.org/10.1097/00004836-200301000-00013
70. Fadhel M, Patel S, Liu E et al (2019) Saccharomyces cerevisiae fungemia in a critically ill patient with acute cholangitis and long term probiotic use. Med Mycol Case Rep 23:23–25. https://doi.org/10.1016/j.mmcr.2018.11.003
71. Izawa S, Inoue Y, Kimura A (1996) Importance of catalase in the adaptive response to hydrogen peroxide: analysis of acatalasaemic Saccharomyces cerevisiae. Biochem J 320(1):61–67. https://doi.org/10.1042/bj3200061
72. Masella R, Di Benedetto R, Varì R et al (2005) Novel mechanisms of natural antioxidant compounds in biological systems: involvement of glutathione and glutathione-related enzymes. J Nutr Biochem 16:577–586
73. Kasemets K, Ivask A, Dubourguier HC, Kahru A (2009) Toxicity of nanoparticles of ZnO, CuO and TiO2 to yeast Saccharomyces cerevisiae. Toxicol In Vitro 23:1116–1122. https://doi.org/10.1016/j.tiv.2009.05.015
74. Sousa CA, Soares HM, Soares EV (2019) Metal (loid) oxide (Al2O3, Mn3O4, SiO2 and SnO2) nanoparticles cause cytotoxicity in yeast via intracellular generation of reactive oxygen species. Appl Microbiol Biotechnol 103:6257–6269
75. Goyal V, Singh A, Singh J et al (2022) Biogenically structural and morphological engineering of Trigonella foenum-graecum mediated SnO2 nanoparticles with enhanced photocatalytic and antimicrobial activities. Mater Chem Phys 282. https://doi.org/10.1016/j.matchemphys.2022.125946
76. Dobrucka R, Dlugaszewska J, Kaczmarek M (2018) Cytotoxic and antimicrobial effect of biosynthesized SnO 2 nanoparticles using Pruni spinosae flos extract. Inorg Nano-Metal Chem 48:367–376. https://doi.org/10.1080/24701556.2019.1569054
77. Haq S, Rehman W, Waseem M et al (2020) Green synthesis and characterization of tin dioxide nanoparticles for photocatalytic and antimicrobial studies. Mater Res Express 7. https://doi.org/10.1088/2053-1591/ab6fa1